

# Geometries and Tautomerism of OHN Hydrogen Bonds in Aprotic Solution Probed by H/D Isotope Effects on $^{13}\text{C}$ NMR Chemical Shifts

Peter M. Tolstoy,<sup>\*,†,‡</sup> Jing Guo,<sup>†</sup> Benjamin Koeppel,<sup>†</sup> Nikolai S. Golubev,<sup>‡</sup> Gleb S. Denisov,<sup>‡</sup> Sergei N. Smirnov,<sup>‡</sup> and Hans-Heinrich Limbach<sup>†</sup>

*Institute of Chemistry and Biochemistry, Free University of Berlin, Germany, and V. A. Fock Institute of Physics, St. Petersburg State University, Russia*

*Received: March 25, 2010; Revised Manuscript Received: August 30, 2010*

The  $^1\text{H}$  and  $^{13}\text{C}$  NMR spectra of 17 OHN hydrogen-bonded complexes formed by  $\text{CH}_3^{13}\text{COOH}(\text{D})$  with 14 substituted pyridines, 2 amines, and *N*-methylimidazole have been measured in the temperature region between 110 and 150 K using  $\text{CDF}_3/\text{CDF}_2\text{Cl}$  mixture as solvent. The slow proton and hydrogen bond exchange regime was reached, and the H/D isotope effects on the  $^{13}\text{C}$  chemical shifts of the carboxyl group were measured. In combination with the analysis of the corresponding  $^1\text{H}$  chemical shifts, it was possible to distinguish between OHN hydrogen bonds exhibiting a single proton position and those exhibiting a fast proton tautomerism between molecular and zwitterionic forms. Using H-bond correlations, we relate the H/D isotope effects on the  $^{13}\text{C}$  chemical shifts of the carboxyl group with the OHN hydrogen bond geometries.

## Introduction

Hydrogen bond interactions of acidic and basic amino acid side chains play an important role in the functions of proteins.<sup>1</sup> The position of the proton in these H-bonds is an important issue as it affects the local electrostatics. Whereas heavy atom positions of crystalline solids can be well determined by X-ray diffraction, the localization of protons in hydrogen bonds often requires the use of neutron diffraction.<sup>2–4</sup> By contrast, for the study of hydrogen bond geometries in noncrystalline solids or in liquids, generally only spectroscopic methods are applicable. They can be used to determine hydrogen bond geometries if appropriate correlations between spectroscopic observables and interatomic distances are available. Such correlations can be either computed theoretically<sup>5–7</sup> or found experimentally.<sup>8–17</sup> For example, the frequency of the  $\nu(\text{OH})$  stretching vibration has been correlated with the O...O and H...O distances in OHO hydrogen bonds.<sup>8</sup> It has also been shown that hydrogen bond geometry correlates with various NMR parameters of AHB hydrogen bonds, such as the chemical shifts of  $^1\text{H}$ ,<sup>9–12</sup> and of heavy atoms A, B =  $^{15}\text{N}$ ,  $^{19}\text{F}$ ,<sup>13–15</sup> and coupling constants across hydrogen bonds  $^1J(\text{AH})$ ,  $^1J(\text{HB})$ , and  $^2J(\text{AB})$ .<sup>13–16</sup> In cases where the hydrogen bond is formed by a  $\text{COOH}/\text{COO}^-$  group, the NMR parameters of the carboxylic carbon could be employed.<sup>9,17</sup>

For example, in a recent series of studies we have studied the OHN hydrogen bond formed between the Asp amino acid side chain of aspartate aminotransferase and its cofactor, pyridoxal phosphate (PLP). The Asp– $\text{COO}^- \cdots \text{HN}^+$ –PLP hydrogen bond in the active site of the enzyme is believed to be essential for the catalysis, while its Asp– $\text{COOH} \cdots \text{N}$ –PLP form seems to be catalytically inactive.<sup>18–20</sup> The experiments performed on the enzyme itself<sup>18</sup> were interpreted using the results of our previous model studies.<sup>19–21</sup> It was shown that the proton position in the H-bond between the Asp and the ring nitrogen atom of the cofactor differs significantly from what would be predicted from the  $\text{p}K_a$  values of the partners. Moreover, the

geometry resembles that of a complex surrounded by a polar aprotic medium.

While establishing correlations for OHN hydrogen bonds, we faced the following problem. In the case of a fast proton tautomerism between the molecular ( $\text{OH} \cdots \text{N}$ ) and the zwitterionic ( $\text{O}^- \cdots \text{HN}^+$ ) forms of the complex, the NMR parameters represent the weighted average of two intrinsic values. As a result, it is difficult to distinguish the spectral manifestations of the proton displacement in the hydrogen bond and the shift of the tautomeric equilibrium.<sup>21</sup> In ref 21, a combined analysis of proton and nitrogen chemical shifts was used to detect the presence of tautomerism. In this paper we apply this approach to the  $^{13}\text{C}$  NMR parameters of the carboxylic group participating in the OHN bridge. This can be advantageous when  $^{15}\text{N}$  NMR data are not available. Unfortunately, the carboxylic carbon chemical shifts of carboxylic acids are strongly influenced by the local chemical structure, and it is difficult to separate contributions from chemical changes and changes of hydrogen bond geometries or proton tautomerism.<sup>22</sup> The values of isotope effects on carboxyl chemical shifts seem to be of a better diagnostic value concerning H-bond geometry as contributions of acid residues cancel. Thus, Perrin et al. have studied one-bond  $^{18}\text{O}$  isotope effect on carboxylic chemical shifts,  $^1\Delta\text{C}(\text{O}) \equiv \delta(\text{C}^{18}\text{OOH}) - \delta(\text{C}^{16}\text{OOH})$ , of acid–base complexes in organic solvents.<sup>23–25</sup> They were able to obtain information regarding hydrogen bond symmetry in solution, in particular about the form of the potential, single- or double-well. However, these effects are small and difficult to measure in the case of biomolecules. Another NMR parameter which seems to be of a high diagnostic value is the two-bond H/D isotope effect on carboxylic chemical shift,  $^2\Delta\text{C}(\text{D}) \equiv \delta(\text{C}^{13}\text{OOD}) - \delta(\text{C}^{13}\text{OOH})$ .<sup>26</sup> Up to now, it has been difficult to obtain such effects from first-principle calculations, as the calculation of the potential energy and shielding surfaces is required.<sup>27–29</sup> An alternative could be experimental studies of model systems. Thus, some of us have recently studied H/D isotope effects on carboxyl chemical shifts in a series of neutral and anionic OHO hydrogen-bonded self-associates of acetic and chloroacetic acids.<sup>9,30</sup> We established a continuous 1D correlation between the average proton positions

<sup>†</sup> Free University of Berlin.

<sup>‡</sup> St. Petersburg State University.

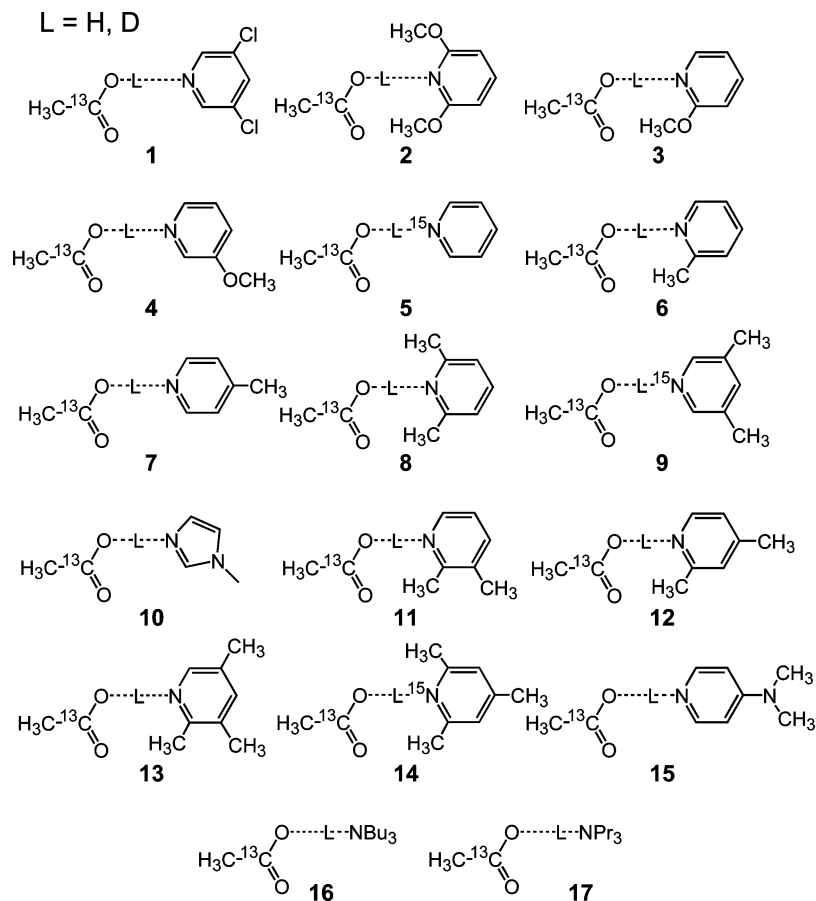


**Figure 1.** Schematic structures of the 17 intermolecular hydrogen-bonded complexes of acetic- $^{13}\text{C}$  acid and nitrogen bases studied in this work. Atomic charges are omitted.

in H-bonds and the values of H/D isotope effects on carboxylic carbon chemical shifts.

In this work we have determined the values of  $^2\Delta\text{C(D)}$  for the case of the OHN hydrogen bonds between 1- $^{13}\text{C}$  labeled acetic acid and nitrogen bases. All studied complexes featured the same carboxylic acid in order to minimize chemical contributions other than hydrogen bonding. We have selected 17 nitrogen bases which all form 1:1 complexes with acetic acid in an aprotic mixture of liquefied gases,  $\text{CDF}_3/\text{CDF}_2\text{Cl}$ . The complexes were studied by low-temperature  $^1\text{H}$  and  $^{13}\text{C}$  NMR spectroscopy. The structures of the complexes are schematically shown in Figure 1. Three nitrogen bases were labeled with  $^{15}\text{N}$  (pyridine- $^{15}\text{N}$ , 3,5-dimethylpyridine- $^{15}\text{N}$ , and 2,4,6-trimethylpyridine- $^{15}\text{N}$ ), which allowed us to measure  $^1J(\text{COHN})$  coupling constants. To detect H/D isotope effects, acetic acid was partially deuterated in the carboxylic group.

## Experimental Section

**Sample Preparation.** Commercially available acetic acid specifically  $^{13}\text{C}$ -enriched in the carboxylic group site (99% 1- $^{13}\text{C}$ , Deutero GmbH) was used for the experiments. Deuteration of acetic- $^{13}\text{C}$  acid was achieved by passing a stream of gaseous  $\text{DCl}$ , obtained as a product of the reaction of 96%  $\text{D}_2\text{SO}_4$  (99.5% D, Deutero GmbH) with dry solid  $\text{NaCl}$ , through a solution of acetic acid- $^{13}\text{C}$  in  $\text{CH}_2\text{Cl}_2$ . All nonlabeled bases were purchased from Aldrich and used without further purification.  $^{15}\text{N}$ -labeled bases were synthesized in our lab. Pyridine- $^{15}\text{N}$  and 2,4,6-trimethylpyridine- $^{15}\text{N}$  were prepared and purified according to recipes available in refs 31 and 32. 3,5-Dimethylpyridine- $^{15}\text{N}$  was synthesized according to ref 33.

Chemicals were weighed and placed into thick-walled NMR sample tubes equipped with PTFE valves (Wilmad, Buena). The solvent,  $\text{CDF}_3/\text{CDF}_2\text{Cl}$  (freezing point below 100 K), prepared by modified method adapted from ref 34, was added to the samples by vacuum transfer. The overall concentration of the acetic acid in the samples, estimated by measuring the volume of the solution at low temperatures (around 120 K), was about 0.02 M. To avoid the formation of intermolecular complexes involving two or more molecules of acetic acid, the bases were added in excess. The usual concentrations of these bases were about 0.04 M in all cases.

**NMR Measurements.** The Bruker AMX-500 NMR spectrometer was equipped with a low-temperature probe which allowed us to perform experiments down to 100 K.  $^1\text{H}$  and  $^{13}\text{C}$  NMR chemical shifts were measured using  $\text{CHF}_2\text{Cl}$  ( $\text{CDF}_2\text{Cl}$ ) as internal standard and converted to the conventional TMS scale. For the measurement of  $\{^1\text{H}\}^{13}\text{C}$  NMR spectra, we used the inverse-gated decoupling scheme, which allowed us to integrate the signals in the  $^{13}\text{C}$  NMR spectra and to attribute signals to the different isotopologs.

**Nomenclature.** Throughout this paper we will use the following nomenclature: chemical shifts are labeled as  $\delta(\underline{\text{COLN}})$ , where the observed nucleus is underlined and  $\text{L} = \text{H, D}$ . A similar nomenclature is used for the  $^1\text{H}-^{15}\text{N}$  spin-spin coupling constants, which are labeled as  $^1J(\underline{\text{COHN}})$ .

**Hydrogen Bond Correlations.** It has been shown by neutron scattering that for an OHN hydrogen bond, the  $\text{O}\cdots\text{H}$  distance  $r_1$  and the  $\text{H}\cdots\text{N}$  distance  $r_2$  are interdependent. $^{2-4}$  This dependence has been originally expressed as

$$p_1 + p_2 = 1 \quad (1)$$

where  $p_1$  and  $p_2$  were defined as

$$p_1 = \exp\left(-\frac{r_1 - r_1^\circ}{b_1}\right); \quad p_2 = \exp\left(-\frac{r_2 - r_2^\circ}{b_2}\right) \quad (2)$$

Parameters  $r_1^\circ$ ,  $r_2^\circ$ ,  $b_1$ , and  $b_2$  have been obtained by the fitting of the experimental data.<sup>2-4</sup> Values of  $p_1$  and  $p_2$  are known as “valence bond orders”.<sup>35</sup> Equations 1 and 2 have been proven valid for weak and medium–strong H-bonds. However, careful analysis of the neutron diffraction data has shown that these equations are not sufficient to describe the geometry of short H-bonds,<sup>36</sup> for which they overestimate the asymmetry of the proton position. Besides, eqs 1 and 2 are unable to describe the differences in the average ground-state geometry of OHN and ODN hydrogen bonds, which are believed to arise from the anharmonicity of the proton potential. In order to account for these problems, the definitions of the valence bond orders have been empirically modified in refs 12, 37, and 38.

$$\begin{aligned} p_{1L} &= p_{1L}^* - 2d^L p_1 (p_{1L}^* p_{2L}^*)^g = \exp(-(r_{1L} - r_1^\circ)/b_1) \\ p_{2L} &= p_{2L}^* - 2d^L p_2 (p_{1L}^* p_{2L}^*)^g = \exp(-(r_{2L} - r_2^\circ)/b_2) \\ p_{1L}^* &= p_1 - c^L (p_1 p_2)^f (p_1 - p_2) \\ p_{2L}^* &= p_2 - c^L (p_1 p_2)^f (p_1 - p_2) \end{aligned} \quad (3)$$

Here, L = H, D. Parameters  $c^L$ ,  $d^L$ ,  $f$ , and  $g$  have been found by fitting in ref 37 and collected in Table 1. The set of eqs 1–3 determines the interdependence between  $r_{1L}$  and  $r_{2L}$ , which have the meaning of vibrationally corrected average O...L and L...N distances. For practical reasons it is often convenient to discuss the hydrogen bond geometry in terms of coordinates

$$q_{1L} = (r_{1L} - r_{2L})/2 \quad \text{and} \quad q_{2L} = r_{1L} + r_{2L} \quad (4)$$

Equations 1–4 cannot be solved analytically to give  $q_{2L}$  as a function of  $q_{1L}$ . Instead, the dependence can be drawn parametrically, which will be done in the Discussion section.

It has been demonstrated that the valence bond orders  $p_{1H}$  and  $p_{2H}$  can be correlated with various NMR parameters.<sup>37</sup> For the  $\delta(\text{COHN})$  chemical shift the following expression has been found valid

$$\delta(\text{COHN}) = \delta_{\text{OH}}^\circ p_{1H} + \delta_{\text{HN}}^\circ p_{2H} + \Delta_{\text{H}}(4p_{1H}p_{2H})^m \quad (5)$$

where  $\delta_{\text{OH}}^\circ$  and  $\delta_{\text{HN}}^\circ$  are the limiting chemical shifts for the free monomeric carboxylic acid and the free protonated base, respectively, and  $\Delta_{\text{H}}$  is the excess parameter, which describes the deviation of  $\delta(\text{COHN})$  for the shortest OHN bond from the average of  $\delta_{\text{OH}}^\circ$  and  $\delta_{\text{HN}}^\circ$ . Similar correlations have previously been applied to the OHO,<sup>9</sup> NHN,<sup>37a</sup> OHN,<sup>37b</sup> FHF,<sup>14</sup> and FHN<sup>15</sup> bonds.

In this work we propose for the first time to use the following equation connecting the <sup>13</sup>C NMR chemical shift of the carboxylic carbon to the bond orders

$$\delta(\underline{\text{COLN}}) = \delta_{\text{free}}^\circ + \delta_{\text{span}}^\circ(1 - p_{1L}) + 4\Delta_{\text{C}}p_{1L}p_{2L} \quad (6)$$

where  $\delta_{\text{free}}^\circ$  is the chemical shift of the “free” (nonbonded) carboxylic group,  $\delta_{\text{span}}^\circ$  is the change of the carboxylic carbon chemical shift upon deprotonation, and  $\Delta_{\text{C}}$  is the excess parameter. The eq 6 itself and the numerical values of the parameters were obtained by fitting the experimental data as described in the Discussion section.

## Results

**<sup>1</sup>H Spectra at 110 K.** In Figure 2 the low-field parts of the <sup>1</sup>H and {<sup>1</sup>H}<sup>13</sup>C NMR spectra of the samples containing 0.02 M of partially deuterated acetic-<sup>13</sup>C acid (CH<sub>3</sub><sup>13</sup>COOH/D) and approximately double excess of the selected bases, dissolved in CDF<sub>3</sub>/CDF<sub>2</sub>Cl, are shown. All spectra were measured at 110 K. The complete set of spectra can be found in the Supporting Information. In each <sup>1</sup>H NMR spectrum an intensive line can be seen, which was attributed to the bridging proton in the 1:1 complex formed by acetic acid and the corresponding nitrogen base. The signals of complexes **9** and **14** are split into doublets due to the <sup>1</sup>J(COHN) spin–spin coupling. For the complex of acetic acid with pyridine-<sup>15</sup>N (**5**), this splitting is apparently below 10 Hz, and thus it is not resolved. The deuterium fraction  $x_{\text{D}}$  in the hydrogen bridge was estimated comparing the relative integrated intensity of the bridging proton signal to that of the CH<sub>3</sub> group of acetic acid. The <sup>1</sup>H NMR chemical shifts measured for all complexes and various temperatures and the values of  $x_{\text{D}}$  are collected in Table 2.

**<sup>13</sup>C Spectra at 110 K.** In the <sup>13</sup>C NMR spectra of complexes **1**, **3**, **5**, **7**, **9**, **11**, and **13** measured at 110 K (Figure 2b), two signals of carboxylic carbons are visible. The ratio of their relative integrated intensities coincides with  $x_{\text{D}}$ , obtained from <sup>1</sup>H NMR spectra. Thus, the <sup>13</sup>C lines were attributed to the carboxylic carbons in the deuterated and nondeuterated forms of the complexes, i.e.,  $\delta(\underline{\text{CODN}})$  and  $\delta(\underline{\text{COHN}})$ , marked “D” and “H” in Figure 2b, respectively. To confirm this assignment, test measurements of the nondeuterated samples have been performed for selected complexes, and in the corresponding {<sup>1</sup>H}<sup>13</sup>C NMR spectra the high-field line was missing. In the <sup>13</sup>C NMR spectra of complexes **14**, **15**, and **17**, only a single signal of carboxylic carbon is visible, indicating that for these complexes  $\delta(\underline{\text{CODN}}) - \delta(\underline{\text{COHN}}) \approx 0$  within the precision of our measurements. All measured <sup>13</sup>C NMR parameters are collected in Table 2.

**Temperature Dependence of <sup>1</sup>H and <sup>13</sup>C NMR Parameters of Complexes 1–17.** Both <sup>1</sup>H and <sup>13</sup>C NMR signals of complexes **1–17** show some temperature dependence (with exception of complex **14**, for which the temperature dependence has not been measured). To illustrate this, the temperature dependency for complex **12** is shown in Figure 3. Upon lowering the temperature from 150 to 103 K, the bridging proton signal of **12** moves to the lower field by about 1.6 ppm. The corresponding signal of the carboxylic carbon moves to the low field by about 1.7 ppm, and the value of H/D isotope effect,  $\delta(\underline{\text{CODN}}) - \delta(\underline{\text{COHN}})$ , changes from –0.56 to –0.22 ppm.

**Isomerism of the Acetic Acid–Methoxypyridine Complex 3.** In most of the studied cases, the <sup>1</sup>H and <sup>13</sup>C NMR spectra show narrow spectral lines. The only exception is complex of

**TABLE 1: Parameters of the Geometric Hydrogen Bond Correlations for OLN Bonds (L = H, D) Used in This Paper**

$r_1^\circ/\text{\AA}$	$b_1/\text{\AA}$	$r_2^\circ/\text{\AA}$	$b_2/\text{\AA}$	$f$	$g$	$c^{\text{H}}$	$d^{\text{H}}$	$c^{\text{D}}$	$d^{\text{D}}$
0.96	0.361	0.992	0.385	5	2	360	0.6	50	0.3

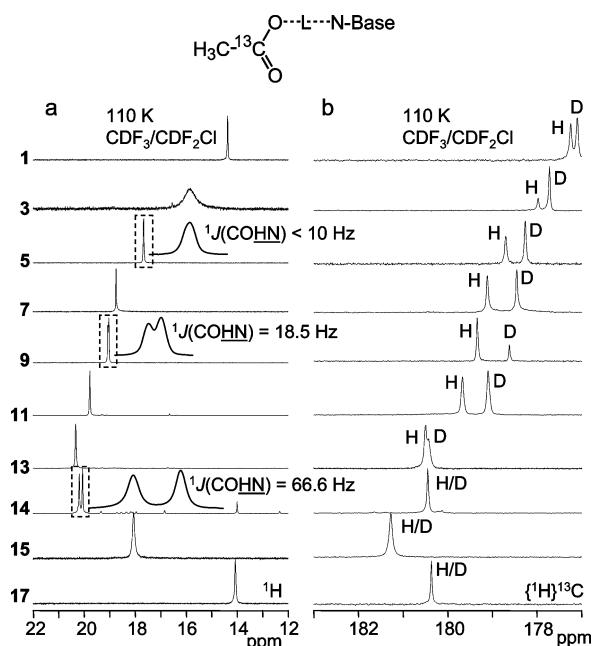


**Figure 2.** Low-field parts of the  $^1\text{H}$  (a) and  $\{^1\text{H}\}^{13}\text{C}$  (b) NMR spectra of the samples containing  $\sim 0.02$  M of partially deuterated in mobile proton sites acetic- $^{13}\text{C}$  acid and  $\sim 0.04$  M of the corresponding base, dissolved in  $\text{CDF}_3/\text{CDF}_2\text{Cl}$  mixture. All spectra were measured at 110 K.

acetic acid with 2-methoxypyridine, for which the bridging proton signal is noticeably broadened. At the same time, there is no additional broadening in the  $^{13}\text{C}$  spectrum. This broadening in  $^1\text{H}$  spectra was found to be independent of the absolute concentration of the sample and of the excess amount of 2-methoxypyridine in the sample (spectra not shown). This means that the broadening is due to the slowing down of some motion within the complex. Furthermore, broadening is absent for other studied pyridines of similar proton-accepting abilities (see, for example, complexes **1**, **4**, and **5**), and it is also absent in case of the symmetrically substituted 2,6-dimethoxypyridine (complex **2**) (spectra of complexes **2** and **4** can be found in the Supporting Information). Though it is hard to be certain about the process which leads to the broadening of the proton signal, one plausible degree of freedom is the rotation around the C–OCH<sub>3</sub> bond (we are grateful to the reviewer for pointing this out). The barrier for such motion in free 2-methoxypyridine is around 4.6 kcal/mol.<sup>39</sup>

## Discussion

We have measured the  $^1\text{H}$  and  $^{13}\text{C}$  NMR spectra of 17 acid–base complexes formed by acetic acid with nitrogen bases dissolved in  $\text{CDF}_3/\text{CDF}_2\text{Cl}$  mixture. At low temperatures (110 K) the slow proton and hydrogen bond exchange regime was reached, which allows one to observe NMR parameters of the complexes, not averaged by the breaking and reforming of the complexes. The observed spectroscopic changes allowed us to number complexes **1–17**, so that the order reflects the overall proton transfer from O to N. The order of  $\text{p}K_a$  values of the bases does not fully coincide with the order **1–17**; see Table 2. This is due to the fact that a base in a hydrogen-bonded complex formed in aprotic medium shows different proton-accepting ability than an isolated base dissolved in aqueous solution.

**Presence of the Proton Tautomerism in the Series.** We start our analysis with Figure 4, where the experimental values

of  $\delta(\underline{\text{COHN}})$  (Figure 4a) and isotope effect  $\delta(\underline{\text{CODN}}) - \delta(\underline{\text{COHN}})$  (Figure 4b) are plotted versus  $\delta(\underline{\text{COHN}})$  for complexes **1–17**. The overall trend of the carboxylic carbon signals is the downfield shift from ca. 177 ppm to ca. 180 ppm upon the increase of the proton chemical shifts. After the  $\delta(\underline{\text{COHN}})$  passes its maximum (this approximately corresponds to the shortest, most symmetric H-bond), the  $\delta(\underline{\text{COHN}})$  becomes rather insensitive to the H-bond geometry (upper branch of the solid curve, which will be explained below). The temperature dependencies for individual complexes do not lie on one curve and form individual linear sets indicated by the dashed lines. The higher the temperature, the closer the experimental data point to the bottom branch of the solid curve, the finding which will be explained in the next section. In the same series, the isotope effect values  $\delta(\underline{\text{CODN}}) - \delta(\underline{\text{COHN}})$  first increase by the absolute value upon the increase of the proton chemical shifts, then rapidly drop to 0 when  $\delta(\underline{\text{COHN}})$  approaches 20 ppm and stay 0 within the margin of the experimental error for complexes with proton transfer. The data points for the weaker complexes,  $\delta(\underline{\text{COHN}}) < 17$  ppm (**1–4**), are lying on the solid correlation curve, while for stronger hydrogen bonds,  $\delta(\underline{\text{COHN}}) > 17$  ppm (especially for **11**, **12**, **13**), the isotope effects start to scatter and show very strong temperature dependency.

The scattering of the points indicates that the model of the continuous proton displacement from O to N is not applicable to the whole series **1–17**. Indeed, as it was mentioned in the Hydrogen Bond Correlations section, the continuous shift of the bridging proton would manifest itself in the continuous shift of the individual spectroscopic parameters (see, for example, eqs 5 and 6), and thus there should be a continuous correlation between any given pair of spectroscopic measurables. This also holds true for the temperature dependencies, because the temperature affects the chemical shifts of an H-bonded complex indirectly, through the geometric changes.

As we see in Figure 4, there is no continuous correlation between  $\delta(\underline{\text{COHN}})$  and  $\delta(\underline{\text{COHN}})$  or  $\delta(\underline{\text{CODN}}) - \delta(\underline{\text{COHN}})$ , and a new model should be constructed to explain the data points. This could be done considering the onset of a proton tautomerism between molecular ( $\text{OH}\cdots\text{N}$ ) and zwitterionic ( $\text{O}^-\cdots\text{HN}^+$ ) forms within the complexes (Figure 5). The possibility of such tautomerism in complexes of carboxylic acids with pyridines has been known for decades.<sup>24,40,41</sup> In the next section we discuss the validity and implications of this model.

**Continuous Proton Transfer versus Two-State Proton Tautomerism.** In some previous publications we have analyzed the spectroscopic dependencies in a series of carboxylic acid–pyridine complexes in terms of a continuous proton displacement from the donor to the acceptor.<sup>16,42,43</sup> In this study (as well as in ref 20, which deals with an intramolecular OHN bond), we demonstrate the presence of a proton tautomerism. So how do these two descriptions fit together? We believe that for many strong hydrogen bonds these two points of view are not in a strict contradiction, and each of them describes a part of the reality. In order to demonstrate this, let us consider Figure 6, in which the hydrogen bond geometries are shown for a series of hypothetical OHN complexes (atomic charges are omitted for simplicity).

For a relatively weak O–H...N hydrogen bond, which is not subject to a proton tautomerism (Figure 6a), the change of the proton-donating ability of OH or of the proton-accepting ability of N would lead to a continuous change of the proton position. The geometric change can also be induced by the change of the local environment, such as temperature-dependent solvent polarity. For a stronger OHN bond the  $\text{OH}\cdots\text{N} \rightleftharpoons \text{O}^-\cdots\text{HN}^+$

TABLE 2:  $pK_a$  Values of Bases, Deuteration Ratios  $x_D$ , and Experimentally Measured NMR Parameters for Complexes 1–17

no.	$pK_a^a$	$x_D$	T/K	$^1J(\text{COHN})/\text{Hz}$	$\delta(\text{COHN})/\text{ppm}$	$\delta(\underline{\text{COHN}})/\text{ppm}$	$\delta(\underline{\text{CODN}})/\text{ppm}$	$\delta(\underline{\text{CODN}}) - \delta(\text{COHN})/\text{ppm}$
1	0.67–0.75	0.60	107		14.400	177.279	177.127	–0.152
			110		14.377	177.258	177.112	–0.147
2	1.60	0.80	110		14.992	177.966	177.794	–0.172
			115		14.931	177.885	177.713	–0.172
3	3.28	0.80	110		15.872	177.986	177.734	–0.253
			120		15.645	177.794	177.551	–0.243
4	4.78	0.45	110		16.991	178.426	178.072	–0.354
			120		16.852	178.239	177.905	–0.334
			130		16.725	178.047	177.730	–0.317
			140		16.594	177.855	177.552	–0.303
5	5.21–5.42	0.60	110	<10	17.669	178.709	178.274	–0.435
			120	<10	17.470	178.461	178.057	–0.404
6	5.96–6.06	0.70	110		18.583	178.906	178.310	–0.597
			120		18.289	178.644	178.087	–0.556
			130		18.023	178.391	177.875	–0.516
			140		17.779	178.178	177.703	–0.475
			150		17.566	177.966	177.578	–0.394
7	5.94–6.10	0.55	110		18.748	179.119	178.461	–0.657
			120		18.439	178.836	178.239	–0.597
8	6.64	0.65	105		19.088	179.331	178.603	–0.728
			110		18.910	179.179	178.482	–0.698
			115		18.744	179.048	178.371	–0.677
			120		18.587	178.906	178.269	–0.637
			125		18.439	178.765	178.158	–0.607
			130		18.296	178.644	178.057	–0.587
			135		18.154	178.522	177.966	–0.556
			140		18.025	178.409	177.875	–0.526
			145		17.905	178.290	177.794	–0.496
9	6.00–6.14	0.25	110	18.5	19.055	179.346	178.628	–0.718
			120	15.7	18.717	179.038	178.381	–0.657
10	7.25	0.35	110		19.171	179.422	178.674	–0.748
			120		18.907	179.149	178.451	–0.698
11	6.48–6.57	0.60	106		19.955	179.856	179.323	–0.537
			110		19.781	179.669	179.089	–0.581
			115		19.603	179.479	178.872	–0.607
			120		19.415	179.288	178.673	–0.615
			131		19.011	178.909	178.294	–0.615
			140		18.694	178.623	178.025	–0.598
			150		18.386	180.413	180.191	–0.222
12	6.64–6.85	0.70	103		20.386	180.413	180.191	–0.222
			105		20.345	180.352	180.100	–0.253
			110		20.194	180.150	179.806	–0.344
			115		20.022	179.938	179.503	–0.435
			120		19.846	179.725	179.230	–0.495
			125		19.669	179.533	178.987	–0.546
			130		19.484	179.351	178.775	–0.576
			140		19.121	178.987	178.391	–0.597
			150		18.790	178.674	178.118	–0.556
13	–	0.40	110		20.334	180.328	180.258	–0.069
			115		20.230	180.146	179.981	–0.165
			120		20.115	179.947	179.687	–0.260
			130		19.873	179.624	179.238	–0.386
			140		19.535	179.229	178.744	–0.485
14	7.25	0.35	110		19.218	178.893	178.339	–0.555
			150		20.131	180.413	180.413	<0.01 <sup>b</sup>
			150		20.131	180.413	180.413	<0.01 <sup>b</sup>
15	9.60–9.61	0.60	110	66.6	18.060	181.283	181.283	<0.01 <sup>b</sup>
			120		18.150	181.171	181.171	<0.01 <sup>b</sup>
16	8.6	0.45	110		14.053	180.413	180.413	<0.01 <sup>b</sup>
			120		14.047	180.423	180.423	<0.01 <sup>b</sup>
			140		14.275	180.387	180.387	<0.01 <sup>b</sup>
17	10.66	0.30	110		14.078	180.372	180.372	<0.01 <sup>b</sup>
			120		14.160	180.383	180.383	<0.01 <sup>b</sup>
			130		14.243	180.373	180.373	<0.01 <sup>b</sup>

<sup>a</sup> Collected from Perrin, D. D. *Dissociation Constants of Organic Bases in Aqueous Solution*, Suppl. 1972; Butterworths: London, 1972. <sup>b</sup> By the absolute value.

tautomerism sets in, and the change of the environment (temperature) or the proton-donating/accepting abilities of the partner molecules would lead simultaneously to the shift of the equilibrium and to the continuous change of the intrinsic

geometry of each individual tautomer (Figure 6b). In the series of structures shown in Figure 6b, from top to bottom the population of tautomers is redistributed toward the zwitterionic structures (depicted as different sizes of “H”), while the

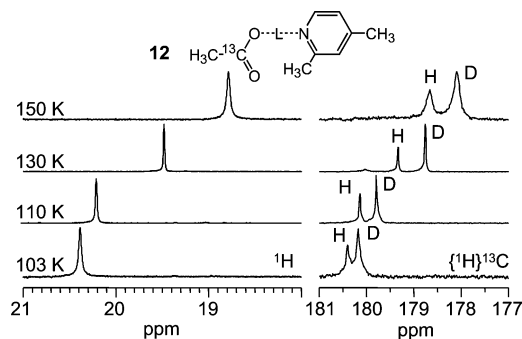


**Figure 3.** Temperature dependence of the low-field parts of the  $^1\text{H}$  and  $\{^1\text{H}\}^{13}\text{C}$  NMR spectra of the sample containing  $\sim 0.02$  M of partially deuterated in mobile proton sites acetic- $^{13}\text{C}$  acid and  $\sim 0.04$  M of 2,4-dimethylpyridine (**12**), dissolved in  $\text{CDF}_3/\text{CDF}_2\text{Cl}$  mixture.

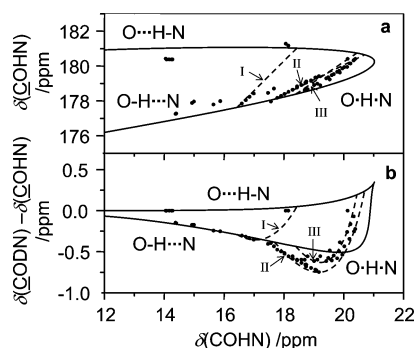


**Figure 4.** Experimentally measured (a) carboxylic carbon chemical shifts and (b) H/D isotope effects on them plotted versus bridging proton chemical shifts for complexes **1–17**. All values are taken from Table 2. Solid line was obtained by the fitting of hydrogen bond correlations; see text for more details. Dashed lines correspond to the averaged experimental values in the presence of the equilibrium between  $\text{OH}\cdots\text{N}$  and  $\text{O}^-\cdots\text{HN}^+$  tautomers in a given complex. Labels I, II, and III correspond to three sets of parameters, used for the calculation of dashed lines; see Table 3 and text for more details.

**TABLE 3: Intrinsic NMR Parameters of the  $\text{OH}\cdots\text{N}$  and  $\text{O}^-\cdots\text{HN}^+$  Tautomers and the Fractionation Factors  $\varphi$  Used To Create the Dashed Lines I–III in Figures 4 and 6<sup>a</sup>**

	line I	line II	line III
$\delta(\text{COH}\cdots\text{N})$ /ppm	16.438	17.687	18.395
$\delta(\text{CO}^-\cdots\text{HN}^+)$ /ppm	18.440	20.697	20.442
$\delta(\text{COH}\cdots\text{N})$ /ppm	177.628	178.095	178.385
$\delta(\text{CO}^-\cdots\text{HN}^+)$ /ppm	181.023	180.645	180.744
$\delta(\text{COD}\cdots\text{N})$ /ppm	177.335	177.711	177.950
$\delta(\text{CO}^-\cdots\text{DN}^+)$ /ppm	181.073	180.883	180.938
$q_1(\text{COH}\cdots\text{N})$ /Å	-0.252	-0.209	-0.183
$q_1(\text{CO}^-\cdots\text{HN}^+)$ /Å	0.213	0.085	0.107
$q_2(\text{COH}\cdots\text{N})$ /Å	2.640	2.603	2.584
$q_2(\text{CO}^-\cdots\text{HN}^+)$ /Å	2.624	2.542	2.551
$\varphi$	0.8	0.4	0.5

<sup>a</sup> See text for more details.

geometry of molecular tautomer gets more symmetric and that of the zwitterionic one gets less symmetric. Naturally, the two-state equilibrium model is an approximation. In reality the given complex might be present in solution as a distribution of many different “solvatomers”, interconverting rapidly (nanosecond time scale) due to the thermal motion of the solvent molecules.<sup>25,44</sup> Thus, such an ensemble can be described by two point geometries only to a certain extent.<sup>21</sup> Lastly, for the hydrogen bonds with complete proton transfer (Figure 6c), there is only one tautomer left, and the further increase of the proton-donating ability of OH, proton-accepting ability of B, or local polarity

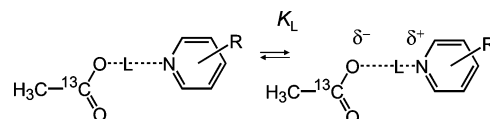


**Figure 5.** Schematic representation of the proton tautomerism between molecular and zwitterionic forms in 1:1 hydrogen-bonded complex formed by acetic acid and substituted pyridine.

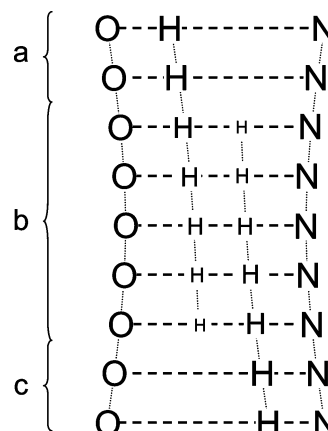


**Figure 6.** Schematic representation of the overall proton transfer pathway in a series of hypothetical OHN hydrogen-bonded complexes subject to proton tautomerism: (a)  $\text{OH}\cdots\text{N}$  tautomer dominates; (b) shift of the tautomeric equilibrium between molecular and zwitterionic forms with the simultaneous change of the intrinsic geometries of tautomers; (c)  $\text{O}^-\cdots\text{HN}^+$  tautomer dominates.

leads to the continuous changes of the geometry of the zwitterionic structure.

In view of the proton transfer pathway schematically described in Figure 6, the experimental series presented in this work allows the following interpretation. In complexes **1–4** the molecular tautomer  $\text{OH}\cdots\text{N}$  dominates, and the spectroscopic changes (including temperature effects) could be explained assuming the continuous shift of the single proton position (the data points in Figure 4 lie close to the solid correlation curve). In complexes **5–15**, which have  $^1\text{H}$  chemical shift above 17 ppm, a tautomeric equilibrium between molecular and zwitterionic forms is clearly detected as a scattering of the data points in Figure 4 away from the correlation curve. The equilibrium is quite sensitive to the properties of the surrounding medium. For example, increase of the solvent polarity by lowering temperature led to almost complete proton transfer from molecular to zwitterionic form in complex **12**. Lastly, for complexes **16** and **17** the zwitterionic tautomer  $\text{O}^-\cdots\text{HN}^+$  dominates, and a continuous shift of the bridging proton can be considered.

#### Hydrogen Bond Correlations and Proton Tautomerism.

Here we analyze the data using hydrogen bond correlations as described in the Experimental section. Equations 3–5 allow us to link  $q_{2\text{H}}$ ,  $\delta(\text{COHN})$ ,  $\delta(\text{COHN})$ , and  $\delta(\text{CODN}) - \delta(\text{COHN})$  values with  $q_{1\text{H}}$ . The resulting curves are depicted in Figure 7a–d as solid lines. The following parameters have been used for the fitting of  $^1\text{H}$  NMR data:  $\delta_{\text{OH}}^{\text{o}} = 6$  ppm,<sup>45</sup>  $\delta_{\text{HN}}^{\text{o}} = 10.5$  ppm,  $\Delta_{\text{H}} = 16$  ppm, and  $m = 1.2$ . For the fitting of  $^{13}\text{C}$  NMR data, we have used  $\delta_{\text{free}}^{\text{o}} = 174.3$  ppm,  $\delta_{\text{span}}^{\text{o}} = 6.5$  ppm,<sup>22,46</sup> and  $\Delta_{\text{C}} = 2.5$  ppm. This set of parameters determines the dependence of the  $\delta(\text{COHN})$  on the  $\delta(\text{COHN})$ , shown in Figure 4a as a solid line, which corresponds to the intrinsic NMR parameters, not averaged by the proton tautomerism. Here we show that the proton tautomerism allows one to explain qualitatively the scattering pattern of the data points in Figure

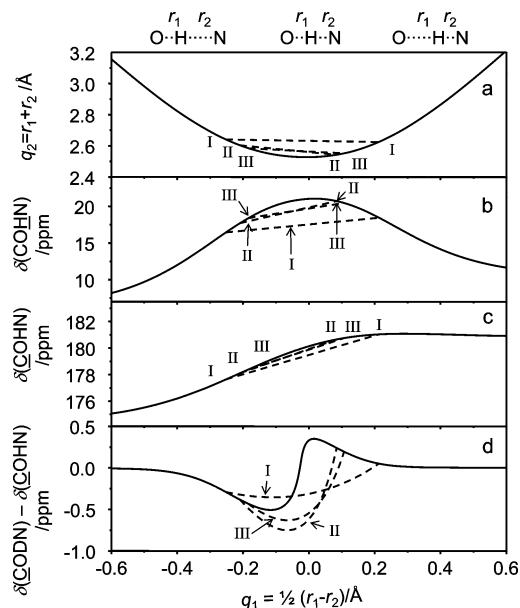


**Figure 7.** Hydrogen bond correlations for OHN hydrogen bonds studied in this paper as functions of  $q_{1H}$ : (a)  $q_{2H}$ ; (b)  $\delta(\text{COHN})$ ; (c)  $\delta(\text{COHN})$ ; (d) H/D isotope effect on carboxylic carbon chemical shift,  $\delta(\text{CODN}) - \delta(\text{COHN})$ . For further explanation, see text.

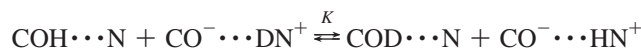
4a, b. As the intrinsic NMR parameters of the tautomers are not known, we have to make some simplifications. In this analysis we will neglect the temperature dependence of the intrinsic geometry of tautomers.

Consider the data points shown in Figure 4a. The data points measured at higher temperatures are located close to the solid line, as the fast equilibrium between molecular and zwitterionic forms is shifted more toward the  $\text{OH}\cdots\text{N}$  tautomer, while points measured at low temperatures are deviating, indicating that there is a larger contribution of  $\text{O}^-\cdots\text{HN}^+$  tautomer to the experimentally observed averaged chemical shifts. Proton and carbon chemical shifts of two tautomers are averaged with the same weight coefficients, which gives a straight (dashed) line in Figure 4a.

Now consider the Figure 4b. Scattering of the H/D isotope effects on NMR chemical shifts is not along the straight lines due to the isotope effect on equilibrium (fractionation). Indeed, for a given complex the equilibrium constant between molecular and zwitterionic forms depends on the bridging particle, H or D. The averaged  $^1\text{H}$  and  $^{13}\text{C}$  NMR chemical shifts can be calculated using the following equations<sup>47</sup>

$$\begin{aligned} \delta_{\text{av}}(\text{COHN}) &= \frac{1}{K_{\text{H}} + 1} \delta(\text{COH}\cdots\text{N}) + \\ &\frac{K_{\text{H}}}{K_{\text{H}} + 1} \delta(\text{CO}^-\cdots\text{HN}^+) \delta_{\text{av}}(\text{CODN}) = \\ &\frac{1}{K_{\text{D}} + 1} \delta(\text{COD}\cdots\text{N}) + \frac{K_{\text{D}}}{K_{\text{D}} + 1} \delta(\text{CO}^-\cdots\text{DN}^+) = \\ &\frac{1}{\varphi K_{\text{H}} + 1} \delta(\text{COD}\cdots\text{N}) + \frac{\varphi K_{\text{H}}}{\varphi K_{\text{H}} + 1} \delta(\text{CO}^-\cdots\text{DN}^+) \quad (7) \end{aligned}$$

where  $K_{\text{H}}$  and  $K_{\text{D}}$  are equilibrium constants for the proton and deuteron tautomerism, correspondingly, and four values of  $\delta$  are the intrinsic  $^{13}\text{C}$  NMR chemical shift of corresponding tautomers.  $\varphi = K_{\text{D}}/K_{\text{H}} = 1/K$  represents the fractionation factor which is equal to the inverse equilibrium constant  $K$  of the reaction



$K$  may not be equal to 1; the deviations mainly arise from differences of zero-point energies of H and D in the molecular and zwitterionic forms. As a result, the proton enriches in the tautomer exhibiting a smaller separation between the zero-point energy levels for H and D.

Though from the current data it is impossible to find explicitly the intrinsic values of NMR parameters for each tautomer and equilibrium constants  $K_{\text{H}}$  and  $K_{\text{D}}$ , it is possible to describe qualitatively the observed dependencies. The following reasoning should be considered as a guideline, rather than a detailed description. In Figures 4 and 7 we show three dashed curves (labeled I, II, and III) which correspond to three arbitrary selected sets of intrinsic NMR parameters and fractionation factors  $\varphi$  listed in Table 3. The meaning of these curves is as follows: when the tautomeric equilibrium is shifted, the experimental averaged data point moves along the dashed line. We remind the reader that the temperature dependence of the intrinsic NMR parameters has been neglected in this qualitative approach.

For example, the dashed line I describes the equilibrium between tautomers which have the  $^1\text{H}$  NMR chemical shifts  $\delta(\text{COH}\cdots\text{N}) = 16.44$  ppm and  $\delta(\text{CO}^-\cdots\text{HN}^+) = 18.44$  ppm. For this pair of chemical shifts, the estimated  $|q_1|$  values are similar and the fractionation factor was set to 0.8, which is close to 1, the value expected for two H-bonds of the same strength. Dashed lines II and III are connecting NMR parameters and geometries of a moderately strong  $\text{OH}\cdots\text{N}$  bond,  $\delta(\text{COH}\cdots\text{N}) \approx 18$  ppm, and a very strong  $\text{O}^-\cdots\text{HN}^+$  bond,  $\delta(\text{CO}^-\cdots\text{HN}^+) \approx 20.5$  ppm. For these tautomers the fractionations were chosen to be significantly different from 1, namely, 0.4 and 0.5.<sup>16</sup> The selected set of parameters allowed us to generate dashed curves and mimic qualitatively the observed temperature dependencies for  $^{13}\text{C}$  chemical shifts and H/D isotope effect on them.

## Conclusions

Proton tautomerism in OHN hydrogen bonds is a well-established phenomenon<sup>24,40,41,49,49</sup> which is hard to detect by NMR due to the signal averaging. In this work we have analyzed  $^1\text{H}$  and  $^{13}\text{C}$  NMR spectra of intermolecular H-bonded complexes formed between acetic acid and nitrogen bases in aprotic solvent (Figure 1). In order to detect the presence of proton tautomerism, we have used the combination of  $\delta(\text{COHN})$ ,  $\delta(\text{COHN})$  chemical shifts and the  $\delta(\text{CODN}) - \delta(\text{COHN})$  isotope effects. The proton tautomerism could be detected as a scattering of the data points away from the correlation curve which corresponds to the intrinsic (nonaveraged) spectroscopic parameters of the H-bonded complexes. The tautomeric equilibrium appeared to be quite sensitive to the properties of the surrounding medium. For example, increase of the solvent polarity by lowering temperature led to almost complete proton transfer from molecular to zwitterionic form in complex **12**. One of the ways to get more information about the distribution of solvatomers would be to combine NMR spectroscopy with an optical spectroscopy which has a much shorter characteristic time, such as UV-NMR proposed recently.<sup>50</sup> Unfortunately the complexes discussed in this work do not absorb above 250 nm and are not suitable for measurements in the UV-NMR setup.

**Supporting Information Available:** Low-field parts of the  $^1\text{H}$  and  $\{^1\text{H}\}^{13}\text{C}$  NMR spectra of the complexes **1–17** dissolved in  $\text{CDF}_3/\text{CDF}_2\text{Cl}$  mixture (110 K). Selected spectra are shown

in Figure 2. This material is available free of charge via the Internet at <http://pubs.acs.org>.

**Acknowledgment.** This research has been supported by the Deutsche Forschungsgemeinschaft, the Fonds der Chemischen Industrie, and the Russian Foundation of Basic Research.

## References and Notes

- (1) (a) Katz, B. A.; Erlod, K.; Luong, C.; Rice, M. J.; Mackman, R. L.; Sprengeler, P. A.; Spencer, J.; Hataye, J.; Janc, J.; Link, J.; Litvak, J.; Rai, R.; Rice, K.; Sideris, S.; Verner, E.; Young, W. *J. Mol. Biol.* **2001**, *307*, 1451. (b) Northrop, D. B. *Acc. Chem. Res.* **2001**, *34*, 790. (c) Kim, K. S. *Biochemistry* **2002**, *41*, 5300.
- (2) Steiner, T.; Saenger, W. *J. Am. Chem. Soc.* **1992**, *114*, 7123.
- (3) Steiner, T.; Saenger, W. *Acta Crystallogr. B* **1994**, *B50*, 348.
- (4) Steiner, T. *J. Chem. Soc., Chem. Commun.* **1995**, 20, 1331.
- (5) (a) Del Bene, J. E.; Alkorta, I.; Elguero, J. *Magn. Reson. Chem.* **2008**, *46*, 457. (b) Del Bene, J. E.; Perera, S. A.; Bartlett, R. J. *J. Am. Chem. Soc.* **2000**, *122*, 3560.
- (6) Takei, K.; Takahashi, R.; Noguchi, T. *J. Phys. Chem. B* **2008**, *112*, 6725.
- (7) Benedict, H.; Shenderovich, I. G.; Malkina, O. L.; Malkin, V. G.; Denisov, G. S.; Golubev, N. S.; Limbach, H. H. *J. Am. Chem. Soc.* **2000**, *122*, 1979.
- (8) (a) Libowitzki, E. *Monatsh. Chem.* **1999**, *130*, 1047. (b) Emsley, J. *Chem. Soc. Rev.* **1980**, *9*, 91. (c) Mikenda, W. *J. Mol. Struct.* **1986**, *147*, 1. (d) Novak, A. *Struct. Bonding (Berlin)* **1974**, *18*, 177.
- (9) Tolstoy, P. M.; Schah-Mohammed, P.; Smirnov, S. N.; Golubev, N. S.; Denisov, G. S.; Limbach, H. H. *J. Am. Chem. Soc.* **2004**, *126*, 5621.
- (10) Emmler, T.; Gieschler, S.; Limbach, H. H.; Buntkowsky, G. *J. Mol. Struct.* **2004**, *700*, 29.
- (11) Jeffrey, G. A.; Yeon, Y. *Acta Crystallogr., Sect. B* **1986**, *B42*, 410.
- (12) Limbach, H. H.; Tolstoy, P. M.; Pérez-Hernández, N.; Guo, J.; Shenderovich, I. G.; Denisov, G. S. *Isr. J. Chem.* **2009**, *49*, 199.
- (13) Lorente, P.; Shenderovich, I. G.; Golubev, N. S.; Denisov, G. S.; Buntkowsky, G.; Limbach, H. H. *Magn. Reson. Chem.* **2001**, *39*, S18.
- (14) Shenderovich, I. G.; Limbach, H. H.; Smirnov, S. N.; Tolstoy, P. M.; Denisov, G. S.; Golubev, N. S. *Phys. Chem. Chem. Phys.* **2002**, *4*, 5488.
- (15) Shenderovich, I. G.; Tolstoy, P. M.; Golubev, N. S.; Smirnov, S. N.; Denisov, G. S.; Limbach, H. H. *J. Am. Chem. Soc.* **2003**, *125*, 11710.
- (16) Smirnov, S. N.; Benedict, H.; Golubev, N. S.; Denisov, G. S.; Kreevoy, M. M.; Schowen, R. L.; Limbach, H. H. *Can. J. Chem.* **1999**, *77*, 943.
- (17) Gu, Z.; Zambrano, R.; McDermott, A. *J. Am. Chem. Soc.* **1994**, *116*, 6368.
- (18) Sharif, S.; Fogle, E.; Toney, M. D.; Denisov, G. S.; Shenderovich, I. G.; Tolstoy, P. M.; Chan Huot, M.; Buntkowsky, G.; Limbach, H. H. *J. Am. Chem. Soc.* **2007**, *129*, 9558.
- (19) Sharif, S.; Chan Huot, M.; Tolstoy, P. M.; Toney, M. D.; Limbach, H. H. *J. Phys. Chem. B* **2007**, *111*, 3869.
- (20) Sharif, S.; Denisov, G. S.; Toney, M. D.; Limbach, H. H. *J. Am. Chem. Soc.* **2007**, *129*, 6313.
- (21) Golubev, N. S.; Smirnov, S. N.; Tolstoy, P. M.; Sharif, S.; Toney, M. D.; Denisov, G. S.; Limbach, H. H. *J. Mol. Struct.* **2007**, *844–845*, 319.
- (22) Gu, Z.; McDermott, A. *J. Am. Chem. Soc.* **1993**, *115*, 4282.
- (23) Perrin, C. L.; Karri, P. *Chem. Commun.* **2010**, *46*, 481.
- (24) Perrin, C. L.; Lau, J. S.; Ohta, B. K. *Pol. J. Chem.* **2003**, *77*, 1693.
- (25) Perrin, C. L. *Pure Appl. Chem.* **2009**, *81*, 571.
- (26) Smith, R.; Brereton, I. M.; Chai, R. Y.; Kent, S. B. H. *Nat. Struct. Biol.* **1996**, *3*, 946.
- (27) Piana, S.; Sebastiani, D.; Carloni, P.; Parrinello, M. *J. Am. Chem. Soc.* **2001**, *123*, 8730.
- (28) Stare, J.; Jezierska, A.; Ambrožič, G.; Košir, I. J.; Kidrič, J.; Koll, A.; Mavri, J.; Hadži, D. *J. Am. Chem. Soc.* **2004**, *126*, 4437.
- (29) (a) Pietrzak, M.; Shibl, M. F.; Bröring, M.; Kühn, O.; Limbach, H. H. *J. Am. Chem. Soc.* **2007**, *129*, 296. (b) Shibl, M. F.; Pietrzak, M.; Limbach, H. H.; Kühn, O. *ChemPhysChem* **2007**, *8*, 315.
- (30) Schah-Mohammed, P.; Shenderovich, I. G.; Detering, C.; Limbach, H. H.; Tolstoy, P. M.; Smirnov, S. N.; Denisov, G. S.; Golubev, N. S. *J. Am. Chem. Soc.* **2000**, *122*, 12878.
- (31) Whaley, T. W.; Ott, D. G. *J. Labelled Compd. Rad.* **1974**, *10*, 283.
- (32) Balaban, A. T.; Boulton, A. J.; McMahan, D. G.; Baumgarten, G. H. E. *Org. Synth. Coll.* **1973**, *5*, 1112.
- (33) Schubert, M. Synthesis of 15N-3,5-dimethylpyridine and Solid State 15N-NMR Study of the Hydrogen Bonded Complexes Formed with 3,5-Dinitrobenzoic Acid. Master's Thesis, Freie Universität, Berlin, 1995.
- (34) Siegel, J. S.; Anet, F. A. I. *J. Org. Chem.* **1988**, *53*, 2629.
- (35) (a) Pauling, L. *J. Am. Chem. Soc.* **1947**, *69*, 542. (b) Brown, I. D. *Acta Crystallogr., Sect. B* **1992**, *B48*, 553. (c) Dunitz, D. *Philos. Trans. R. Soc. London* **1975**, *B272*, 99.
- (36) (a) Steiner, T. *J. Phys. Chem. A* **1998**, *102*, 7041. (b) Steiner, T.; Majerz, I.; Wilson, C. C. *Angew. Chem.* **2001**, *113*, 2728. (*Angew. Chem., Int. Ed.* **2001**, *40*, 2651). (c) Steiner, T.; Wilson, C. C.; Majerz, I. *Chem. Commun.* **2000**, 1231. (d) Benedict, H.; Limbach, H. H.; Wehlan, M.; Fehlhammer, W.-P.; Golubev, N. S.; Janoschek, R. *J. Am. Chem. Soc.* **1998**, *120*, 2939.
- (37) Limbach, H. H.; Pietrzak, M.; Benedict, H.; Tolstoy, P. M.; Golubev, N. S.; Denisov, G. S. *J. Mol. Struct.* **2004**, *706*, 115.
- (38) Limbach, H. H.; Pietrzak, M.; Sharif, S.; Tolstoy, P. M.; Shenderovich, I. G.; Smirnov, S. N.; Golubev, N. S.; Denisov, G. S. *Chem.—Eur. J.* **2004**, *10*, 5195.
- (39) Cheng, R.-J.; Corey, E. J. *Org. Lett.* **2010**, *12*, 132.
- (40) (a) Barrow, G. M. *J. Am. Chem. Soc.* **1956**, *78*, 5802. (b) Denisov, G. S.; Starosta, J.; Schreiber, V. M. *Opt. Spektrosk.* **1973**, *35*, 447. (c) Golubev, N. S.; Denisov, G. S.; Koltsov, A. I. *J. Mol. Struct.* **1981**, *75*, 333.
- (41) Nasielski, J.; Vander Donckt, E. *Spectrochim. Acta* **1963**, *19*, 1989.
- (42) Golubev, N. S.; Denisov, G. S.; Smirnov, S. N.; Shchepkin, D. N.; Limbach, H.-H. *Z. Phys. Chem.* **1996**, *196*, 73.
- (43) Smirnov, S. N.; Golubev, N. S.; Denisov, G. S.; Benedict, H.; Schah-Mohammed, P.; Limbach, H.-H. *J. Am. Chem. Soc.* **1996**, *118*, 4094.
- (44) Perrin, C. L.; Lau, J. S. *J. Am. Chem. Soc.* **2006**, *128*, 11820.
- (45) (a) Kymtis, L.; Mikulskis, P. *J. Magn. Reson.* **1975**, *20*, 475. (b) Lumbroso-Bader, N.; Couprie, C.; Baron, D.; Govil, G. *J. Magn. Reson.* **1975**, *17*, 386.
- (46) Facelli, J. C.; Gu, Z.; McDermott, A. *Mol. Phys.* **1995**, *86*, 865.
- (47) Sharif, S.; Denisov, G. S.; Toney, M. D.; Limbach, H. H. *J. Am. Chem. Soc.* **2006**, *128*, 3375.
- (48) Hansen, P. E.; Sitkowski, J.; Stefaniak, L.; Rozwadowski, Z.; Dziembowska, T. *Ber. Bunsen-Ges. Phys. Chem.* **1998**, *102*, 410.
- (49) Rozwadowski, Z.; Majewski, E.; Dziembowska, T.; Hansen, P. E. *J. Chem. Soc., Perkin Trans.* **1999**, *2*, 2809.
- (50) Tolstoy, P. M.; Koeppe, B.; Denisov, G. S.; Limbach, H. H. *Angew. Chem., Int. Ed.* **2009**, *48*, 5745.